Symmetry and three-dimensional anisotropy of polar domain boundaries observed in ferroelastic $LaAlO_3$ in the complete absence of ferroelectric instability

H. Yokota,[1,*] S. Matsumoto,[2] E. K. H. Salje,[3] and Y. Uesu[4]

[1]*Department of Physics, Chiba University, 1–33 Yayoi-cho, Inage-ku, Chiba-shi, Chiba 263–8522, Japan*

[2]*Department of Physics, Faculty of Science and Engineering, Chiba University, 1–33 Yayoi-cho, Inage-ku, Chiba-shi, Chiba 263–8522, Japan*

[3]*Department of Earth Sciences, Cambridge University, Downing Street, Cambridge CB2 3EQ, United Kingdom*

[4]*Department of Physics, Faculty of Science and Engineering, Waseda University, 3-4-1 Okubo, Shinjuku-ku, Tokyo 169–8555, Japan*

(Received 19 July 2018; revised manuscript received 27 August 2018; published 13 September 2018)

The domain boundaries of ferroelastic $LaAlO_3$ (LAO) are examined using a nonlinear optical second harmonic generation (SHG) microscope. Although bulk crystalline LAO possesses centro-symmetry and is inherently non-SH active, our three-dimensional observations reveal that the domain boundaries of LAO exhibit SH activity with almost the same magnitude within a boundary. The polarization dependence of the SH intensities shows strong anisotropy, which is explained by the polar trigonal point group, $3m$. The polar direction is found to be along the $[111]_{pc}$ axis and inclined from the domain boundary plane. It implies that the biquadratic coupling scheme of two order parameters could be the main origin of the emergence of polar nature at the domain boundary. Our experimental results together with those of $CaTiO_3$ suggest that the polar nature of the domain boundary in ferroelastic materials may be a ubiquitous phenomenon.

DOI: 10.1103/PhysRevB.98.104105

Ferroic materials are characterized by a hysteresis loop that represents the nonlinear relation between the primary order parameters and the corresponding conjugate fields. The hysteresis loop originates from the switching process of domains with a specific orientation under an applied external field. Without fields, these domains are related to the energetically equivalent domains generated by symmetry lowering. Since the domain structure is often closely related to some important physical properties, many studies have been performed to manipulate the domain structures. One successful example of a functional device using domain structures is a quasi-phase matching (QPM) device of periodically inverted 180° domains [1,2] to obtain highly efficient optical wavelength conversion. In contrast, only in recent works has attention gradually moved to domain boundaries (DBs). Thanks to the development of experimental techniques over the last decade, it has become clear that the DBs exhibit their own physical properties, which is not surprising since DBs could possess different structures from the bulk host and consequently produce large gradient forces. In particular, the electrical transport properties of DBs have been intensively studied in various ferroelectric oxides [3–12], including high conductivity in multiferroic $BiFeO_3$ [3,5,7,8], orientation-depending conductivities in $YMnO_3$ [13], charged DBs [14–22], etc. This research field is now termed "domain boundary engineering" and is expected to pioneer a new frontier in nanoscience [23].

The present study reports the polar nature of DBs in essentially nonpolar ferroelastic, lanthanum aluminum oxide ($LaAlO_3$, abbreviated LAO hereafter). Similar studies have already been performed for $CaTiO_3$ (CTO) and $SrTiO_3$ (STO) using an aberration corrected transmission electron microscope (TEM) [24], a resonant piezoelectric spectroscope (RPS) [25–27] and a second harmonic generation microscope (SHGM) [28,29]. We chose LAO because it is purely ferroelastic in the sense that no ferroelectric instability has been observed, in contrast to CTO and STO, which are known as incipient ferroelectrics, or quantum paraelectrics. Consequently, the latter two easily exhibit ferroelectricity under a small external field. For the DB nature of LAO, a pioneering work was performed very recently that revealed the piezoelectric nature of mechanically stressed LAO using an RPS and a piezo-force microscope [30]. A piezoelectric coefficient comparable to that of quartz crystals was observed. The authors claimed that this large coefficient originates from the complicated, dense tweed pattern of LAO. However, more precisely investigating whether it is a DB effect or an overall effect of a bulk LAO specimen seems to be necessary, since the RPS, which records macroscopic measurements, cannot easily separate these contributions. In this sense, the SHGM has some advantages: an observation can be focused on a DB and its possible point symmetry can be determined from the anisotropy of the SH intensity represented by the two-dimensional (2D) polar diagram. Furthermore, our SHGM is of the confocal scanning type and provides the three-dimensional (3D) images of polar regions, from which we can estimate the polarization direction at each point in a given boundary. Notably, particularly in the case of ferroelastics such as LAO, the polar boundaries can be distinguished by a sharp SHG contrast because neighboring bulk regions are nonpolar and appear pitch black in an SHG image.

A commercially available LAO single crystal with dimensions of $10 \times 10 \times 0.5\,\mathrm{mm}^3$ (K & R Creation) was used for our experiments. We chose a $\langle 001 \rangle_{pc}$-oriented LAO single crystal with $\{1\,0\,0\}_{pc}$ edges as the specimen. Here, pc means the pseudocubic perovskite axis, and all crystallographic

*hiroko.9bq@chiba-u.jp

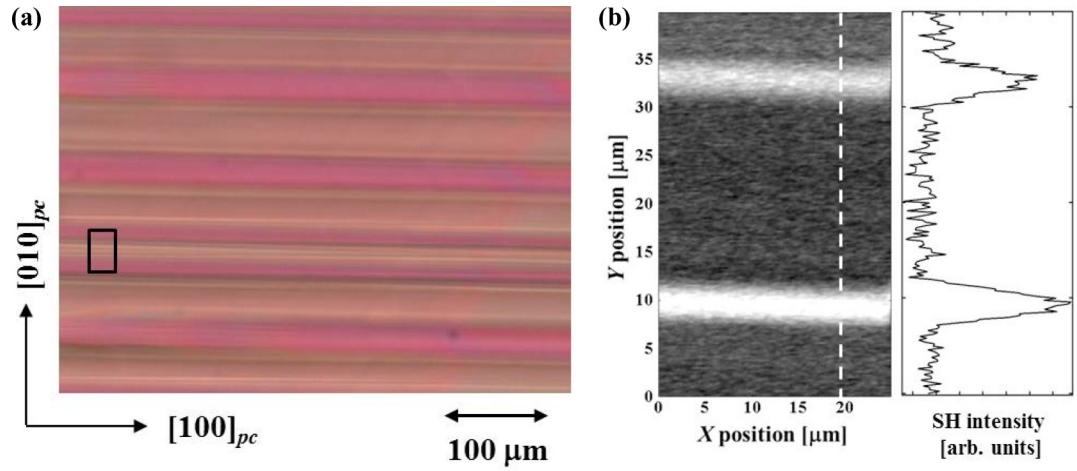

FIG. 1. (a) Polarization microscope image of $LaAlO_3$ under a crossed Nicol configuration. (b) 2D image of SH wave distribution. The area by the SHGM is enclosed by the square in (a). On the right, cross-section 1D plot for a dashed line is shown.

directions refer to these axes. The specimen was first examined using a polarization microscope with a crossed Nicol configuration, and then observed using a transmission type of SHGM. The SHG images were acquired using an Nd : YVO_4 laser with a wavelength of 1064 nm, a repetition frequency of 40 kHz, laser power of 0.125 W, and laser energy of 3.125 μJ. The microscopic configuration was a transmission-type confocal scanning system equipped with a piezo-actuator stage for a lateral plane (XY axes) combined with a stepping-motor stage for the depth direction (the Z axis). SH waves with a wavelength of 532 nm generated from a specimen are selected by a spectrometer, and the intensities are detected point by point by a photomultiplier tube, which is synchronized with incident laser pulses by a lock-in amplifier. More details of our optical system is found in Ref. [28]. The 2D and the 3D SHG images were obtained in nondestructive way with the diffraction limit resolution of 0.5 μm.

Figure 1(a) shows a polarization micrograph of an LAO single-crystal plate. Needlelike domains with a striped pattern aligned parallel to the $[1\,0\,0]_{pc}$ direction are observed throughout the specimen. This type of domain structure is commonly observed in many perovskite ferroelectric and ferroelastic materials, e.g., $BaTiO_3$, STO, and CTO [31,32]. In our specimen, only one type of DB is observed, as shown in this figure. The DBs are within a range of 20 to 40 μm apart. Due to the fine, complex domain structure of our specimen, no clear extinction angle is obtained. Additionally, no distinct tweed microstructure appears, which is substantially different from the previously reported structures in strained LAO [30]. Therefore, we can choose one boundary to precisely analyze the SHGM images.

For SHG measurements, a strong signal is often detected from the surface of a specimen due to symmetry lowering. To avoid this effect, one-dimensional (1D) scanning along the Z axis was performed, and the focus positions were adjusted to be inside the specimen during experiments. Figure 1(b) shows a typical 2D SHG image of the specimen. Polarization directions of the fundamental and SH waves are parallel to each other and are inclined 66° from the X axis. The SH active regions are observed as two bright straight lines parallel to the $[1\,0\,0]_{pc}$ direction, which are clearly silhouetted against the darkness. Due to an extremely weak signal from our specimen (10^{-8} times weaker than that of normal ferroelectrics), a large electric voltage was applied to a photomultiplier tube to attain a detectable intensity. Since applying a large voltage also increases the noise, the signal-to-noise (SN) ratio should be examined to confirm the dependability of the experimental result. The calculated SN ratio in Fig. 1(b) is 10:1. This relatively high SN ratio supports the reliability of the present experiments. The possibility that those bright regions are domains themselves can be eliminated because the space group of LAO at room temperature is centrosymmetric $R\bar{3}c$, and therefore is SH nonactive. To construct the perspective view of the DB structure, the specimen was scanned at different depths with a 4 μm step and the constructed 3D image is shown in Fig. 2. Several SH active lines with uniform brightness are present, which are parallel to each other and almost perpendicular to the sample surface.

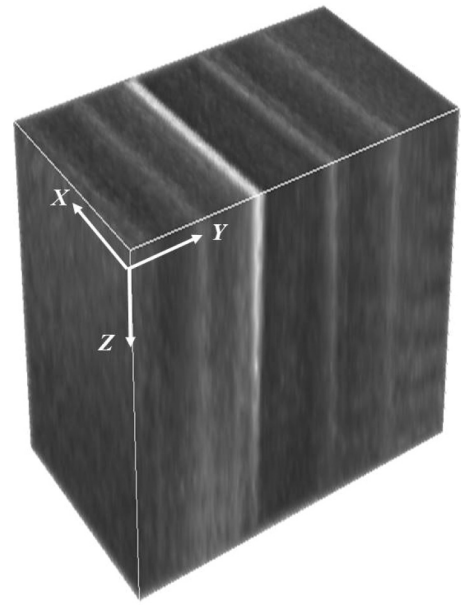

FIG. 2. Constructed 3D SHG image. White planes correspond to the domain boundaries that are SH active.

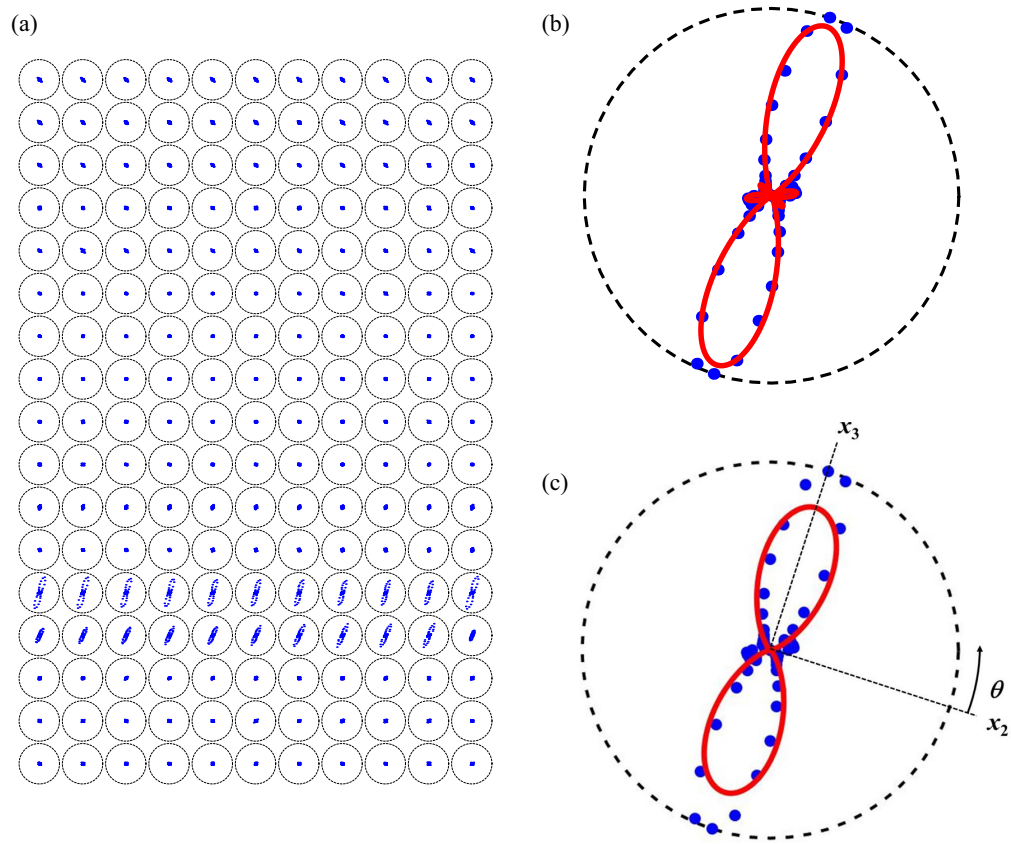

FIG. 3. (a) Polar diagrams mapping of $LaAlO_3$. Fitting results using (b) $3m$ and (c) 32 point groups. Blue dots correspond to the experimental data and the red line to the fitting result.

In ferroelastics, DBs are oriented to satisfy the strain compatibility between two adjacent domains. The orientations of the DBs are theoretically calculated by Sapriel and others [33–35]. According to Ref. [33], the DBs are classified into two categories. One is the so-called W-wall, which is crystallographically prominent. Another type of DB is the W'-wall, whose orientation is determined by the relative magnitude of the second-rank strain tensor components. LAO is an improper ferroelastic with a structural phase transition from cubic $Pm\bar{3}m$ to rhombohedral $R\bar{3}c$ at 813 K [36–38], which can be expressed as $m3mF\bar{3}m$ with the Aizu notation [39]. This class contains 9 DBs, and their orientations can be determined with the following equations:

$$x = 0, \tag{1}$$

$$y = 0, \tag{2}$$

$$z = 0, \tag{3}$$

$$x = \pm y, \tag{4}$$

$$y = \pm z, \tag{5}$$

$$z = \pm x. \tag{6}$$

Here, x, y, and z are the cubic axes, and the triad axis is chosen to be along the $[1\,1\,1]_{pc}$ direction. All DBs belonging to this class are W-walls because the orientations do not depend on the strain tensor. Since the SH active DBs that we observed are parallel to the $[1\,0\,0]_{pc}$ direction and perpendicular to the $[0\,0\,1]_{pc}$ plane, the plane equation is expressed as $y = 0$.

To clarify the polar nature at the DB, determining the point group is essential. Among the 32 point groups, 21 classes are noncentrosymmetric. These point groups, except for the point group 432, are all SH and piezo active but only 10 of them belong to the polar class. Therefore, to determine whether a sample is polar or nonpolar, the piezoelectric response is not sufficient, and the determination of the point group is a more direct way. SHG is suitable for this purpose since it originates from the third-rank d tensor components, and the anisotropy of SH intensities directly reflects the point symmetry. The SH anisotropy of the LAO specimen was measured with the polarization directions of the fundamental and SH waves being parallel. The 2D SH images were taken with different polarizations, and the 2D images were divided into several hundred small grids to average the SH intensity in each grid and construct the polar diagram mapping. The polar diagram mapping was performed over the same area as that in Fig. 1(b), and the obtained results are shown in Fig. 3(a). Except for the DBs, no SH intensity is detected from the specimen in any polarization directions. At the DB, the distribution of SH intensity exhibits the anisotropy with two maxima shown in Fig. 3(b). Additionally, a small local maximum is observed approximately 65° away from the

maxima. Although the intensities are different, the shape of the SH anisotropy and the directions of the SH maxima are similar for each DB, which is different from the case of CTO. For CTO, the directions of the SH maxima are different among the neighboring DBs, possibly because in CTO, adjacent DBs are closer than those of LAO, and the polarizations interact with each other to reduce the energy by slightly changing the polar direction. Since the $R\bar{3}c$ is SH inactive, we assume that the symmetry of the DB is lower than that of the bulk and fit the data with several different point groups. The best fitting is attained with trigonal $3m$ assuming that the triad axis lies in the direction of the SH maxima. This presumption is reasonable since the magnitude of the d tensor component is empirically proportional to the spontaneous polarization. The nonlinear polarization P related to the SHG can be expressed as

$$P_i = d_{ijk} E_j E_k, \tag{7}$$

where E is the electric field of the fundamental wave and each of i, j, and k represent the direction of polarization of the relevant fields and correspond to the principle axes of the crystal [40]. Since d_{ijk} is symmetrical in j and k, subscript j and k are replaced in a single suffix l running from 1 to 6, which is known as the Voigt notation or the matrix notation [41]. Using the Voigt notation, Eq. (7) can be rewritten as

$$\begin{pmatrix} P_1 \\ P_2 \\ P_3 \end{pmatrix} = \begin{pmatrix} d_{11} & d_{12} & d_{13} & d_{14} & d_{15} & d_{16} \\ d_{21} & d_{22} & d_{23} & d_{24} & d_{25} & d_{26} \\ d_{31} & d_{32} & d_{33} & d_{34} & d_{35} & d_{36} \end{pmatrix} \begin{pmatrix} {E_1}^2 \\ {E_2}^2 \\ {E_3}^2 \\ E_2E_3 \\ E_3E_1 \\ E_1E_2 \end{pmatrix}. \tag{8}$$

For $3m$, there are eight nonzero d tensor components. Among them, four are independent, and the associated matrix can be described using the Voigt notation as follows:

$$\begin{pmatrix} 0 & 0 & 0 & 0 & d_{15} & -2d_{22} \\ -d_{22} & d_{22} & 0 & d_{15} & 0 & 0 \\ d_{31} & d_{31} & d_{33} & 0 & 0 & 0 \end{pmatrix}. \tag{9}$$

Here, the triad axis being parallel to the $[111]_{pc}$ direction corresponds to the x_3 direction. In our experimental geometry, $E_1 = 0$, $E_2 = \cos\theta$, $E_3 = \sin\theta$, where θ is the polarization direction from the x_2 that is perpendicular to the triad axis x_3 [see Fig. 3(c)]. Therefore, the SH intensity is fitted with the following equation:

$$I \propto [\{d_{22}\cos^2\theta + d_{15}\cos\theta\sin\theta\}\cos\theta + \{d_{31}\cos^2\theta + d_{33}\sin^2\theta\}\sin\theta]^2. \tag{10}$$

The SH intensity is well known to also depend on the coherence length, which is different for each d tensor component. Here, we assume that the coherence length is the same for all d tensor components. As a result of the fitting procedure, the relative magnitudes of the d tensor components are obtained as $d_{15} : d_{22} : d_{31} : d_{33} = 11.1 : 1 : 11.1 : -18.7$. Note that we treat these four d tensor components independently and the same values are obtained for d_{15} and d_{31} without any restrictions during the analysis. Since this finding is consistent with Kleinman's law, which is commonly proven for nonlinear optical transparent crystals, this experimental evidence suggests the validity of our analysis. The fitting result using $3m$ is shown as a red solid line in Fig. 3(b), which reproduces the experimental results well, and the small lobes observed between the two ovoids are well fitted with this model. For comparison, a fitting result using the nonpolar point group 32 is shown in Fig. 3(c). Clearly, this point group does not reproduce the experimental result well. These results suggest that the point group of LAO DB is trigonal $3m$. Toledano *et al.* theoretically deduced the symmetry of DBs in ferroelectrics and ferroelastics from their organic relationship with the primary transition order parameter [42]. According to their calculations, the symmetry of the DBs of LAO is either mmm or $\bar{3}m$, which contradicts our experimental results. In the case of ferroelastics, the primary order parameter, which is the tilt of the octahedron, always preserves the inversion symmetry. Therefore, it gives the DB an intrinsic nonpolar nature, which indicates that the one-order parameter model does not sufficiently explain the polar nature at the ferroelastic DB. This finding is consistent with the theoretical simulation of CTO, which needs the off-centering of a Ti atom being the secondary order parameter to obtain the polarization at the domain wall [43]. The polarization direction of the LAO DBs is uniquely determined as the $[111]_{pc}$ direction because $3m$ belongs to the uniaxial group. In the case of CTO, Van Aert *et al.* observed that the displacement of the Ti ion creates a polarization parallel to the DB [24], which is not the case for LAO. The polarization has both parallel and perpendicular projection components along the DB direction. This result is important to understand the origin of the polarity at the DB. To elucidate the origin of the polar nature at the DBs, many numerical calculations have been performed. An improper origin arising from a cooperative interplay of rotational distortions is proposed based on first-principal calculations [44]. A linear flexoelectricity [45] has been considered as one of the main contributors to the local polarization at the DB. However, these origins only allow possessing either a parallel or perpendicular projection component along the DB. On the other hand, any polarization directions are permitted by a biquadratic coupling [46,47], which contains a rotopolar coupling to the gradients of the antiferrodistortive oxygen tilts and a trilinear coupling. Our experimental result suggests that the polar nature at the domain boundary originates from the biquadratic coupling.

A geometrical picture of the tensor component is the best way to visualize the anisotropy of physical properties. Indicatrix is an example of the representation quadric of the second-rank tensor. Although it is not as simple as the second-rank tensor component, it is possible to visualize the anisotropy of the third-rank tensor by quadric surfaces. Since the relative magnitude of all independent d tensor components are obtained from the analysis, we can construct the representation surface of the nonlinear optical coefficients for LAO DBs as shown in Fig. 4(a). The radius vector in the arbitrary direction represents the magnitude of the d tensor component along its direction. The obtained quadratic surface exhibits a strong anisotropy with an almond shape on top of the tripod plate. The almond shape is mainly composed of the d_{33} component and is along the $[111]_{pc}$ direction. A tripod plate

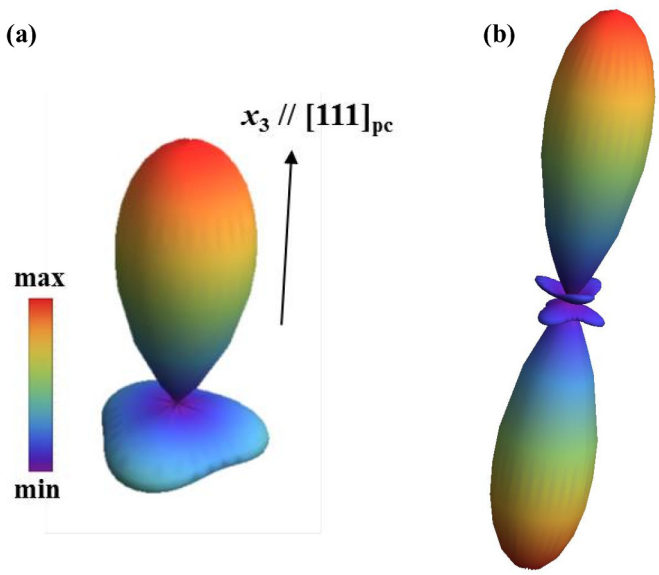

FIG. 4. (a) Nonlinear optical surface plot of $LaAlO_3$ representing the three-fold symmetry along the $[111]_{pc}$ direction. (b) The 3D SH intensity distribution plot constructed from the experimental results. The color code represents the magnitude of the d tensor component and SH intensity.

is linked to the three-fold axis and is the main contribution of the d_{15} component. Since the SH intensity is proportional to the square of the nonlinear polarization, we can construct the 3D representation of SH polarimetry from the nonlinear optical surface. The experimental polarization dependence of the SH intensity looking down from an arbitrary direction is obtained as the intersection of a 3D representation of SH polarimetry and the plane that is normal to the arbitrary direction. Figure 4(b) exhibits the 3D SH intensity distribution plot of LAO. At the end of the two lobes, two three-petaled lobes appear with upwards and downwards orientation. These petals reflect the three-fold symmetry that possesses three maxima. The orientations of these maxima differ from each other by 60°. Therefore, the magnitude of these petals depends on the observation direction, and our experimental results clearly demonstrate this tendency.

Since $3m$ is one of the polar classes, we conclude that the DB of LAO is polar and possibly ferroelectric in the sense that its polarity can be switched by applying stress or an electric field. Further experiments are in progress to confirm the switching behavior.

The polar nature of purely ferroelastic LAO with no ferroelectric instability was examined using an SHGM. We revealed that ferroelastic DBs in LAO are SH active inside the specimen. Analyzing the anisotropy of the SH intensity leads us to the conclusion that the point group of the DBs of LAO is trigonal $3m$ and belongs to the polar class. The polarization direction of the LAO DB is determined, and the relative values of all independent d tensor components are obtained. In contrast with ferroelastic $CaTiO_3$, the polarization orientation is not parallel to the DB. It suggests that the polar nature at the DB in LAO originates from the biquadratic coupling of the order parameters.

H.Y. is grateful to JPSJ KAKENHI for financial support (Grants No. 15K17674 and No. 17K05489). H.Y. acknowledges support from the Murata Science Foundation through Grant No. AN17029. E.K.H. thanks the Leverhulme trust (EM-2016-004).

[1] J. A. Armstrong, N. Bloembergen, J. Ducuing, and P. S. Pershan, Phys. Rev. **127**, 1918 (1962).
[2] M. M. Fejer, G. A. Magel, D. H. Jundt, and R. L. Byer, IEEE J. Quantum Electron. **28**, 2631 (1992).
[3] J. Seidel, L. W. Martin, Q. He, Q. Zhan, Y.-H. Chu, A. Rother, M. E. Hawkridge, P. Maksymovych, P. Yu, M. Gajek, N. Balke, S. V. Kalinin, S. Gemming, F. Wang, G. Catalan, J. F. Scott, N. A. Spaldin, J. Orenstein, and R. Ramesh, Nat. Mater. **8**, 229 (2009).
[4] S. Y. Yang, J. Seidel, S. J. Byrnes, P. Shafer, C.-H. Yang, M. D. Rossell, P. Yu, Y.-H. Chu, J. F. Scott, J. W. Ager, L. W. Martin, and R. Ramesh, Nat. Nanotechnol. **5**, 143 (2010).
[5] J. Seidel, P. Maksymovych, Y. Batra, A. Katan, S.-Y. Yang, Q. He, A. P. Baddorf, S. V. Kalinin, C.-H. Yang, J.-C. Yang, Y.-H. Chu, E. K. H. Salje, H. Wormeester, M. Salmeron, and R. Ramesh, Phys. Rev. Lett. **105**, 197603 (2010).
[6] Y. Kim, M. Alexe, and E. K. H. Salje, Appl. Phys. Lett. **96**, 032904 (2010).
[7] P. Maksymovych, J. Seidel, Y. H. Chu, P. Wu, A. P. Baddorf, L.-Q. Chen, S. V. Kalinin, and R. Ramesh, Nano Lett. **11**, 1906 (2011).
[8] S. Farokhipoor and B. Noheda, Phys. Rev. Lett. **107**, 127601 (2011).
[9] J. Guyonnet, I. Gaponenko, S. Gariglio, and P. Paruch, Adv. Mater. **23**, 5377 (2011).
[10] P. Maksymovych, A. N. Morozovska, P. Yu, E. A. Eliseev, Y.-H. Chu, R. Ramesh, A. P. Baddorf, and S. V. Kalinin, Nano Lett. **12**, 209 (2012).
[11] Q. He, C.-H. Yeh, J.-C. Yang, G. Singh-Bhalla, C.-W. Liang, P.-W. Chiu, G. Catalan, L. W. Martin, Y.-H. Chu, J. F. Scott, and R. Ramesh, Phys. Rev. Lett. **108**, 067203 (2012).
[12] T. Sluka, A. K. Tagantsev, D. Damjanovic, M. Gureev, and N. Setter, Nat. Commun. **3**, 748 (2012).
[13] T. Choi, Y. Horibe, H. T. Yi, Y. J. Choi, W. Wu, and S.-W. Cheong, Nat. Mater. **9**, 253 (2010).
[14] B. M. Vul, G. M. Guro, and I. I. Ivanchik, Ferroelectrics **6**, 29 (1973).
[15] C.-L. Jia, S.-B. Mi, K. Urban, I. Vrejoiu, M. Alexe, and D. Hesse, Nat. Mater. **7**, 57 (2008).
[16] N. Balke, M. Gajek, A. K. Tagantsev, L. W. Martin, Y.-H. Chu, R. Ramesh, and S. V. Kalinin, Adv. Funct. Mater. **20**, 3466 (2010).
[17] Y. Du, X. L. Wang, D. P. Chen, S. X. Dou, Z. X. Cheng, M. Higgins, G. Wallace, and J. Y. Wang, Appl. Phys. Lett. **99**, 252107 (2011).

[18] P. Zubko, S. Gariglio, M. Gabay, P. Ghosez, and J.-M. Triscone, Annu. Rev. Condens. Matter Phys. **2**, 141 (2011).
[19] Y. Qi, Z. Chen, C. Huang, L. Wang, X. Han, J. Wang, P. Yang, T. Sritharan, and L. Chen, J. Appl. Phys. **111**, 104117 (2012).
[20] W. Wu, Y. Horibe, N. Lee, S.-W. Cheong, and J. R. Guest, Phys. Rev. Lett. **108**, 077203 (2012).
[21] L. Li, P. Gao, C. Nelson, Y. Zhang, S.-J. Kim, A. Melville, C. Adamo, D. Schlom, and X. Pan, Microsc. Microanal. **19**, 1654 (2013).
[22] T. Sluka, A. K. Tagantsev, P. Bednyakov, and N. Setter, Nat. Commun. **4**, 1808 (2013).
[23] E. K. H. Salje, ChemPhysChem **11**, 940 (2010).
[24] S. Van Aert, S. Turner, R. Delville, D. Schryvers, G. Van Tendeloo, and E. K. H. Salje, Adv. Mater. **24**, 523 (2012).
[25] P. Zubko, G. Catalan, A. Buckley, P. R. L. Welche, and J. F. Scott, Phys. Rev. Lett. **99**, 167601 (2007).
[26] J. F. Scott, E. K. H. Salje, and M. A. Carpenter, Phys. Rev. Lett. **109**, 187601 (2012).
[27] E. K. H. Salje, O. Aktas, M. A. Carpenter, V. V. Laguta, and J. F. Scott, Phys. Rev. Lett. **111**, 247603 (2013).
[28] H. Yokota, H. Usami, R. Haumont, P. Hicher, J. Kaneshiro, E. K. H. Salje, and Y. Uesu, Phys. Rev. B **89**, 144109 (2014).
[29] H. Yokota, S. Niki, R. Haumont, P. Hicher, and Y. Uesu, AIP Adv. **7**, 085315 (2017).
[30] E. K. H. Salje, M. Alexe, S. Kustov, M. C. Weber, J. Schiemer, G. F. Nataf, and J. Kreisel, Sci. Rep. **6**, 27193 (2016).
[31] M. Takagi, N. Akaba, and S. Suzuki, J. Phys. Soc. Jpn. **46**, 1811 (1979).
[32] A. Buckley, J. P. Rivera, and E. K. H. Salje, J. Appl. Phys. **86**, 1653 (1999).
[33] J. Sapriel, Phys. Rev. B **12**, 5128 (1975).
[34] V. Janovec and J. Přívratská, in *International Tables for Crystallography* (International Union of Crystallography, Chester, England, 2006), pp. 449–505.
[35] J. Erhart, Phase Transitions **77**, 989 (2004).
[36] C. J. Howard, B. J. Kennedy, and B. C. Chakoumakos, J. Phys.: Condens. Matter **12**, 349 (2000).
[37] H. Lehnert, H. Boysen, J. Schneider, F. Frey, D. Hohlwein, P. Radaelli, and H. Ehrenberg, Z. Kristallogr. - Cryst. Mater. **215**, 536 (2000).
[38] S. A. Hayward, F. D. Morrison, S. A. T. Redfern, E. K. H. Salje, J. F. Scott, K. S. Knight, S. Tarantino, A. M. Glazer, V. Shuvaeva, P. Daniel, M. Zhang, and M. A. Carpenter, Phys. Rev. B **72**, 054110 (2005).
[39] K. Aizu, J. Phys. Soc. Jpn. **28**, 706 (1970).
[40] S. A. Denev, T. T. A. Lummen, E. Barnes, A. Kumar, and V. Gopalan, J. Am. Ceram. Soc. **94**, 2699 (2011).
[41] J. F. Nye, *Physical Properties of Crystals: Their Representation by Tensors and Matrices* (Clarendon Press, Oxford, 1985).
[42] P. Tolédano, M. Guennou, and J. Kreisel, Phys. Rev. B **89**, 134104 (2014).
[43] L. Goncalves-Ferreira, S. A. T. Redfern, E. Artacho, and E. K. H. Salje, Phys. Rev. Lett. **101**, 097602 (2008).
[44] P. Barone, D. Di Sante, and S. Picozzi, Phys. Rev. B **89**, 144104 (2014).
[45] E. K. H. Salje, S. Li, M. Stengel, P. Gumbsch, and X. Ding, Phys. Rev. B **94**, 024114 (2016).
[46] A. Schiaffino and M. Stengel, Phys. Rev. Lett. **119**, 137601 (2017).
[47] B. Casals, A. Schiaffino, A. Casiraghi, S. J. Hämäläinen, D. López González, S. Van Dijken, M. Stengel, and G. Herranz, Phys. Rev. Lett. **120**, 217601 (2018).